



Overlap influence in images obtained by an unmanned aerial vehicle on a digital terrain model of altimetric precision

Nicole Lopes Bento, Professor Gabriel Araújo E Silva Ferraz, Rafael Alexandre Pena Barata, Mr Lucas Santos Santana, Brenon Diennevan Souza Barbosa, Dr Leonardo Conti, Valentina Becciolini & Dr Giuseppe Rossi

To cite this article: Nicole Lopes Bento, Professor Gabriel Araújo E Silva Ferraz, Rafael Alexandre Pena Barata, Mr Lucas Santos Santana, Brenon Diennevan Souza Barbosa, Dr Leonardo Conti, Valentina Becciolini & Dr Giuseppe Rossi (2022) Overlap influence in images obtained by an unmanned aerial vehicle on a digital terrain model of altimetric precision, European Journal of Remote Sensing, 55:1, 263-276, DOI: [10.1080/22797254.2022.2054028](https://doi.org/10.1080/22797254.2022.2054028)

To link to this article: <https://doi.org/10.1080/22797254.2022.2054028>



© 2022 The Author(s). Published by Informa UK Limited, trading as Taylor & Francis Group.



Published online: 11 Apr 2022.



Submit your article to this journal [↗](#)



View related articles [↗](#)



View Crossmark data [↗](#)

Overlap influence in images obtained by an unmanned aerial vehicle on a digital terrain model of altimetric precision

Nicole Lopes Bento^a, Professor Gabriel Araújo E Silva Ferraz^a, Rafael Alexandre Pena Barata^a, Mr Lucas Santos Santana^a, Brenon Diennevan Souza Barbosa^a, Dr Leonardo Conti^b, Valentina Becciolini^b and Dr Giuseppe Rossi^b

^aDepartment of Agricultural Engineering, Universidade Federal de Lavras, Lavras, Brazil; ^bDipartimento di Scienze e Tecnologie Agrarie Alimentari Ambientali e Forestali, DAGRI, Università degli Studi di Firenze, Firenze, Italy

ABSTRACT

Photogrammetric data are systematically used in several segments. Products such as Digital Terrain Models (DTMs) provide detailed surface information, however the geometric reliability of these products is questionable compared to data collected by topographic survey by GNSS RTK. The present research assesses the quality of DTMs obtained using an Unmanned Aerial Vehicle (UAV) with different parameters, overlap percentages, and flight directions, comparing the results to those of the topography method Global Navigation Satellite System – Real-Time Kinematic (GNSS RTK). Were done twelve flight plans with different overlaps (90x90, 80x80, 80x60, 70x50, 70x30, and 60x40%) and directions (transverse and longitudinal to the planting line). The parameters of height (Above Ground Land- AGL) and speed were fixed at 90 m and 3 m/s respectively and a Ground Sample Distance (GSD) of 0,1 m is obtained for all flights. Overall, the flight with 70x50% overlap in the transverse direction generated the best results, with a total processing time of 12 minutes and 17 seconds (about 1.5 hours faster than 90x90%), an Root Mean Square Error (RMSE) 0.589 m, and meets the minimum overlap required by 60x30% aerophotogrammetry; furthermore, the results did not differ statistically from the high overlaps of 90x90% and 80x80%.

ARTICLE HISTORY

Received 30 March 2021
Revised 20 December 2021
Accepted 10 March 2022

KEYWORDS

Precision agriculture; remote sensing; RPAS; UAV

Introduction

The utilization of Unmanned Aerial Vehicle (UAV) has gained prominence in technological applications in several segments of society. This equipment stands out as an emerging technology for photogrammetric data acquisition (Klemas, 2015; Santana et al., 2019). Photogrammetric data offer advantages in agricultural planning and monitoring (Santos et al., 2019; Zisi et al., 2018) due to the high spatial and temporal resolutions of their derived products (Peña et al., 2013; Torres-Sánchez et al., 2014). Compared to photogrammetry planes, UAVs are relatively low in cost and capable of coupling different cameras and sensors (Hashemi-Beni et al., 2018).

The generation of photogrammetric products that present reliable information depends on proper flight planning. Aerial images captured without prior planning can compromise the orthomosaic and Digital Terrain Model (DTM). The orthomosaic corresponds to a single image created by compiling photos using specific software (Torrado et al., 2016) corrected for lens distortion, camera tilt, perspective, and topographic relief. DTM considers the elevation data contained in each pixel and can be used for various applications. This model represents only the terrain

elevation – that is, the ground without buildings, crops, and other features that do not represent the terrain surface (Rumpler et al., 2013; Sopchaki et al., 2018). On the other hand, the Digital Surface Model (DSM) considers the natural cover and buildings in the terrain elevation, not only the terrain elevation itself (Höhle, 2009).

Some studies have addressed the quality and application of the orthomosaics, DEMs, and DTMs derived from UAVs. Uysal et al. (2015) analyzed the generation of DEMs from images acquired by a microcopter. Tamminga et al. (2015), evaluated the quality of a DTM generated by UAV images using limnological characterization. Sopchaki et al. (2018) tested the quality of orthomosaics without ground control points. Thus, the use of UAVs can facilitate fast decision-making based on the slope of the terrain (Pereira et al., 2013).

The production of DTM via the topographic survey (Global Satellite Navigation System Receivers GNSS and Total Station) is still considered a costly and expensive process (Mora et al., 2020). For this reason, the generation of reliable measurements from digital models could provide an alternative to replace or improve classic surveying operations. However, it is

known that the topographic survey method can achieve better positional accuracy compared to photogrammetry. Using techniques and equipment with appropriate calibrations for the photogrammetric data could provide accurate details of the surface. It is noteworthy, however, that there are other MDT generation methods, including airborne photogrammetry and/or lidar, UAV-based lidar, terrestrial laser scanning among others, which however were not evaluated in this study.

UAV DTM with acceptable geometric errors and without georeferenced ground control points can contribute to cost reductions and collection agility. In agriculture, the development of logistical systems (roads and access), simple embankment regions (without design project), and irrigation systems represent examples of operations with low demands for high geometric precision (Aguilar et al., 2005; Burrough & McDonnell, 1998).

Adjustments in the UAV flight plane can enhance the geometric precision of photogrammetric products. The correct definitions of height, overlap, and flight speed are essential to achieve survey efficiency and sufficient photogrammetric quality (Santos et al., 2019). The processing of high-spatial-resolution images may represent a hindrance to large projects. Another significant approach is to assess the influence of the flight direction on the detail and data acquired for the generation of a DTM. A mission planned in the longitudinal direction to the terrain slope may result in acquiring images and elevation data different from those acquired in the transverse direction. Tests with different image overlaps can reduce flight time and image processing (Mesas-Carrascosa et al., 2016).

Thus, there is growing interest in determining the ideal overlap for terrain reconstruction (Dandois et al., 2015; Leachtenauer & Driggers, 2001). Some authors, however, suggest implementing high overlaps as a guarantee of high DTM accuracy (Eisenbeiss, 2009; Rabah et al., 2018; Westoby et al., 2012), reporting that high overlap percentages result in a low vertical Root Mean Square Error (RMSE). However, the present study proposes investigating the influence of different overlaps and their significant effects on altimetric precision, based on best-of-flight and processing time considerations.

Studies on the effects of the technical properties of the flight configuration (overlap and flight direction) used to establish relationships between ground elevation data and UAV-derived aerial imagery data are limited. The presents study seeks to fill these gaps. Eltner et al. (2017) and Hirschmuller (2007) suggest that flight altitude, speed, and trajectory have the greatest influence on the accuracy of the DEM. Smith et al. (2016) indicate the distance of the soil sample (GSD) as an important factor, while Clapuyt et al. (2016) and Leitão et al. (2016) highlight the camera-configuration parameters.

The factors mentioned above are important considerations when designing UAV surveys to support land-survey studies at the civil construction, agricultural, and environmental levels, as such surveys can optimize the development of activities, directly providing time savings, cost reductions, and high-precision results. Therefore, the construction of maps and terrain models by collecting and integrating photographs from different imaging configurations is proposed as an alternative to optimizing land-survey activities.

In this context, it is necessary to obtain an adequate overlap and flight direction to ensure the product quality and increase the UAV's autonomy and data processing efficiency. This study evaluates the quality of DTMs using variations in parameters such as image overlap percentages and flight directions from UAV images compared to topographic surveys performed using GNSS RTK (Global Navigation Satellite System – Real-Time Kinematic) receivers.

Materials and methods

Study area

This study was carried out in an experimental coffee plantation located at the Federal University of Lavras (UFLA), Brazil, covering an area of 2.1 hectares (502,860 and 503,080 m W and parallels 7,652,880 and 7,652,720 m S, in the UTM zone 23S projection and Sirgas 2000) in the municipality of Lavras, Minas Gerais, Brazil (Figure 1). According to the Köppen classification, the climate in this area is humid and temperate, with dry winters and rainy summers (Cwa; Alvares et al., 2013). The average annual rainfall and temperature are 1,530 mm and 19.4°C, respectively (D'Andréa et al., 2009).

Topographic data

The topographic survey by GNSS RTK instrument was performed based on 44 predefined points, creating a grid with a spatial resolution of 25 × 25 m (Figure 1). The points were tracked and fixed in the field in kinematic mode with a margin of error less than 0.03 m using a pair of Spectra precision GNSS antennas, operating in the RTK mode with a base and rover.

In RTK positioning, two receivers are used to collect data continuously. One of the receivers, called the reference station (base), is positioned over a point of known coordinates. The other receiver (mobile receiver) is used to collect data and points of interest for the user and determine the position in real time (Barbosa et al., 2013). The tracking model of the RTK provides high speed and precision in determining the geographical position and ellipsoidal altitude. Therefore,

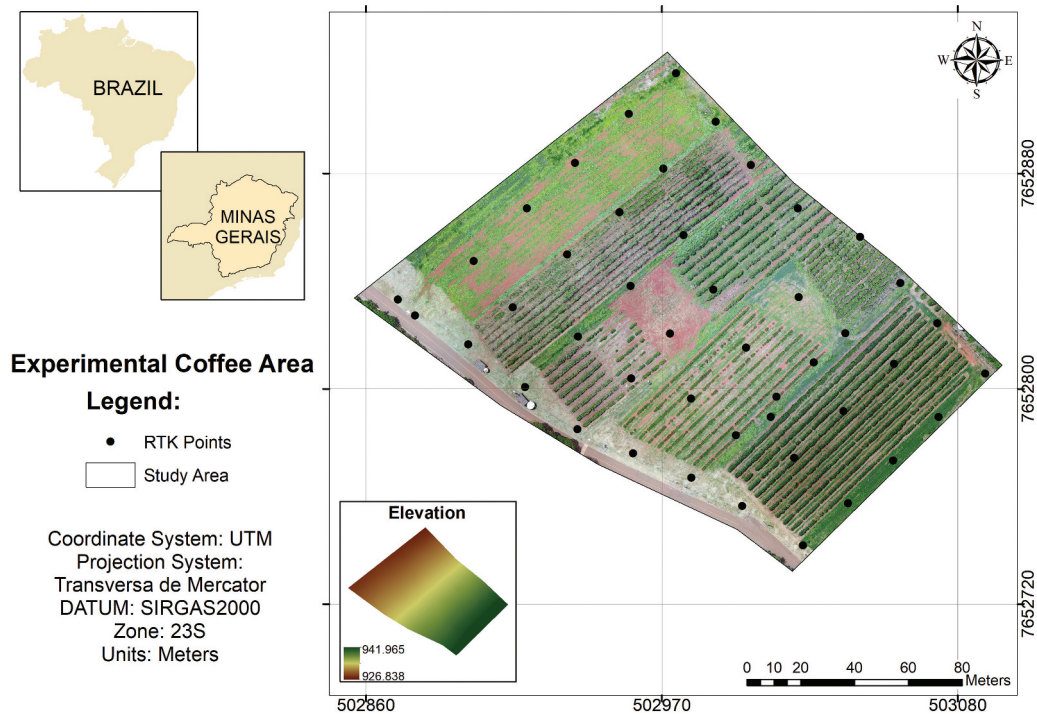


Figure 1. Location map of the study area.

using RTK, using RTK is possible to obtain the geometric unevenness of an alignment with reference to the local geoid (Vitti et al., 2017).

Image acquisition

The images were collected using an UAV DJI Phantom 4 Advanced (DJI, Shenzhen, China) featuring an embedded optical sensor with 20-megapixel RGB CMOS, FOV 84°, a focal length of 8.8/24 mm. The flights were standardized and performed from 11:00 am to 1:00 pm because during this period, the sun reaches its zenith and becomes perpendicular to the terrain surface (Santos et al., 2020), shadows are minimized, and image quality is improved (Silva et al., 2016).

The flight-plan parameters for the study area were defined for different image overlaps and in different flight directions. Twelve flights were performed according to the planning based on the same GSD (0,1 m), height Above Ground Land (AGL-90 m), and flight speed (3 m/s), as outlined in Table 1.

Two flight directions were considered: longitudinal and transverse (Figure 2). For the 80x80%, and 90x90% overlap, the flight was performed only in the longitudinal direction because the sidelap and frontlap were the same, regardless of flight directions.

Coverage of the study area employed different overlaps and flight directions. However, according to the characteristics of the used aircraft battery, only one flight was needed for each configuration to produce a complete image of the studied area. However, for

Table 1. Parameters adopted for the study flights.

Flight number	Overlap (%)	Direction
1	90x90	Longitudinal
2	80x80	Longitudinal
3	80x60	Longitudinal
4	80x60	Transverse
5	70x50	Longitudinal
6	70x50	Transverse
7	70x30	Longitudinal
8	70x30	Transverse
9	60x40	Longitudinal
10	60x40	Transverse
11	60x30	Longitudinal
12	60x30	Transverse

larger areas, and depending on the different flight configurations (overlap, direction, speed, and height), at times necessary to subdivide the study area and carry out more imaging flights to completely reach the area.

Data processing

After the flights were performed, the flow-data process was performed. The processing time for this process was proportional to the processing capacity of the computer used. The computer configurations used in this study are described in Table 2.

Using the Agisoft Photoscan 1.4 software (Agisoft LLC, St. Petersburg, Russia), the spatial references were initially corrected with specifications for SIRGAS 2000 UTM 23S. Afterwards, we proceeded with alignment of the images (triangulation and automatic measurement of crossing points and connections via automatic image correlation), construction of a dense cloud of points, construction of the image

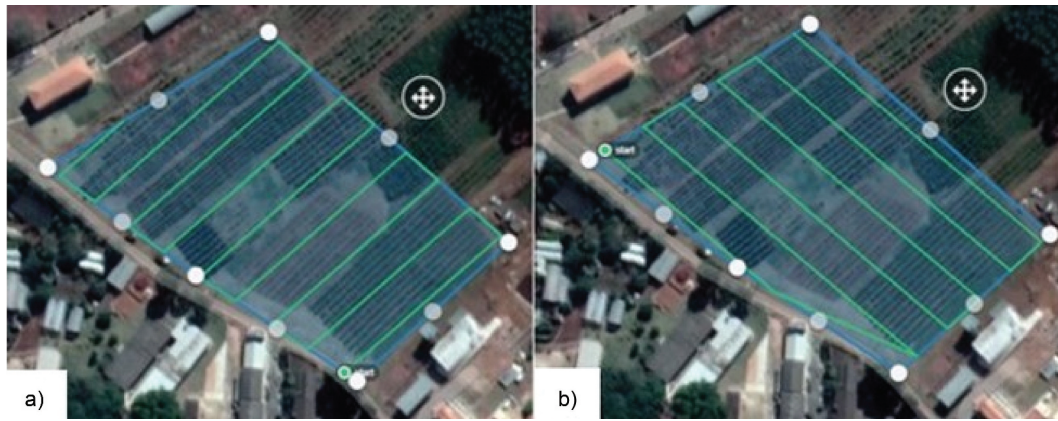


Figure 2. Longitudinal (A) and transverse (B) flight directions.

texture, digital terrain modeling based on the DEM, orthorectification of the images, and production of the final orthomosaic (Figure 3).

The photogrammetric parameters used for the different stages of image processing are described in Table 3. To generate the DTM, semi-automatic classification was performed to exclude vegetation, buildings, and noise from the point cloud via the automatic correlation of images, with configurations also described in Table 3. The specifications were maintained for all overlaps, representing standardized processes and providing a comparative basis for the subsequent results.

The points obtained through the topographic survey (GNSS RTK) were interpolated in the ArcGis 10.1 software (Esri, 2013) to obtain the study surface called “control” (Figure 4). This information was used as the field truth, and the reference was subsequently compared to the surfaces generated by the images captured by the sensor coupled to the UAV. The variation in the elevation of the study area ranged from 926.838 to 941.985 m, with the highest elevation values observed in the south zone and decreasing towards the north, where lower elevation values were observed (Figure 4).

Several contour lines, spaced 1 m apart, were vectorized in the DTMs obtained via the UAV in the ArcGis 10.1 software (Esri, 2013). A central line on the study area was drawn across the contour lines (Figure 4) to study the altimetric profiles. The data

were extracted relative to the AGL altitude of each point, and then we plotted the altimetric profile for each studied DTM based on the crossing points of the standardized contour lines.

The DTMs generated for each overlap and flight direction were standardized, initially by pixel quantity and then, in sequence, by geographic positioning (georeferencing), with both procedures being performed in a GIS environment using the ArcGis 10.1 software (Esri, 2013). The georeferencing was carried out considering the image with the largest overlap (90x90%) and considering information on the

Table 3. Parameters used and their respective settings in agisoft photoscan for the study processes.

Parameters	Settings
Align Photos	
Precision	Highest
Pair preselection	Disable
Build Dense Cloud	
Quality	Medium
Depth filtering	Aggressive
Build Mesh	
Surface Type	Arbitrary
Face count	Medium
Build Texture	
Mapping mode	Generic
Blending mode	Mosaic
Build DEM	
Interpolation	Enable
Source Data	Dense Cloud
Build Orthomosaic	
Mode Combination	Mosaic
Surface	Mesh
Build DTM	
Class	
From	Any Class
Classify Ground Points	
Max Angle (deg)	3.0
Max Distance (m)	1.0
Cell Size (m)	20.0

Table 2. Computer configuration used for data processing.

Item	Configuration
CPU	Intel Core i5- 8250 U @Turbo Boost up 1,6–3,4 GHz
RAM	8 GB
GPU	NVIDIA GeForce MX130

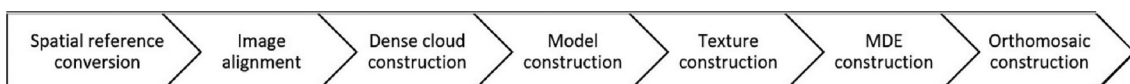


Figure 3. Flow diagram of image processing in Agisoft Photoscan.

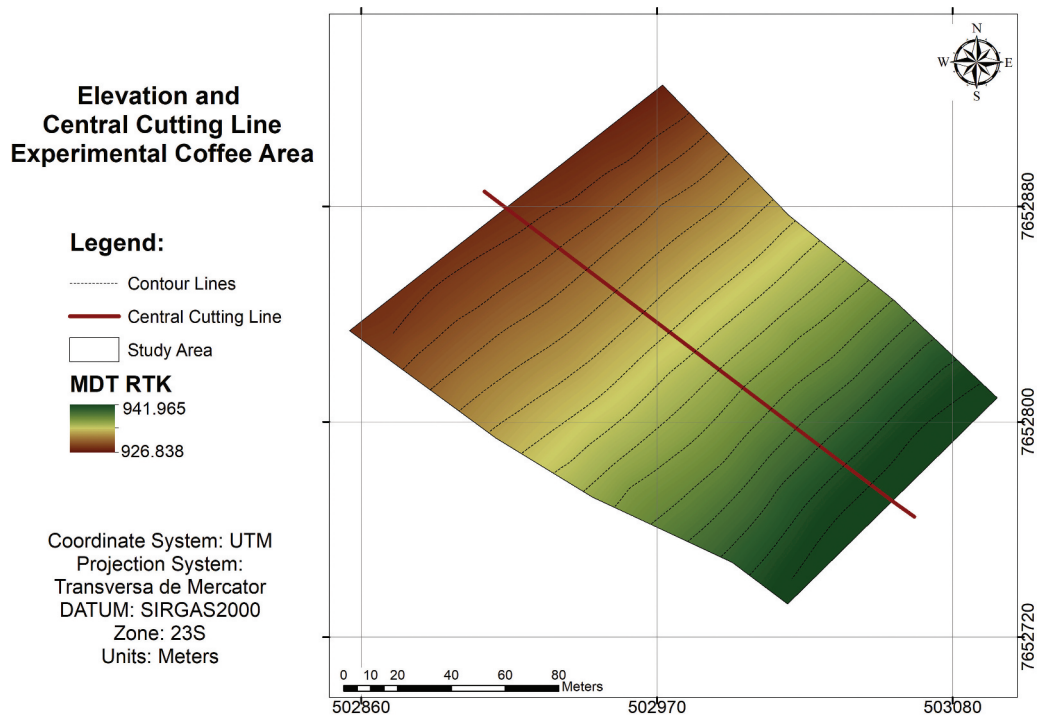


Figure 4. Elevation map based on a survey of the topographic survey (GNSS RTK- control) and delimitation of the central cutting line and contour lines in the survey of the altimetric profile.

similarity of built-up areas in the other overlaps, thus carrying out a drag and adjustment of the horizontal positioning between all the generated products. These procedures were performed primarily to guarantee the correct calculation of pixels on the assessed surfaces, and don't alter information nor interfere with the reliability of the information. Therefore, the present study considers only the deviations and errors related to altitude, excluding errors related to geographical position.

Statistical analysis

The control profile and the other topographic profiles were initially compared by differentiating the line graphs of the topographic profiles. The differences and sums of squares between the DTM produced by the GNSS RTK control profile and the DTMs produced by UAV images, with their respective overlaps, were also obtained to determine the profile with the closest result to the control. Dunnett's (1995) mean comparison test was performed in sequence to determine overlaps that did not differ significantly from the control.

The errors were calculated considering the entire study surface, since the product generated by the UAV is the complete representation of the terrain and, therefore, the interest is to investigate the behavior of the error distribution along the entire study surface. Thus, the surface interpolated with the GNSS RTK data was considered in contrast to the modeled surface in each study flight. Initially,

the Mean Squared Error (MSE; Equation 1) was calculated considering the entire study surface and in sequence pixel by pixel (only squared error) allowing the visualization of the error behavior along the study terrain and later the Root Mean Squared Error (RMSE; Equation 2) which is commonly used to express the accuracy of numerical results, with the advantage of providing error values with the same dimensions as those of the analyzed variables (Hallak & Pereira, 2011). Calculations were performed in a GIS environment, using the "Map Algebra" function of the ArcGis 10.1 software (Esri, 2013).

$$MSE = \frac{\sum_{i=1}^N (A_{is} - A_{ob})^2}{n} \quad (1)$$

$$RMSE = \sqrt{\frac{\sum_{i=1}^N (A_{is} - A_{ob})^2}{n}} \quad (2)$$

where A_{is} is the simulated altitude, and A_{ob} is the observed altitude.

Finally, the agglomerative hierarchical analysis of dendrograms was employed to assess and verify the differences and statistical similarities between the sets of overlaps studied, based on the RMSE values that were determined in the R software (R Development Core Team, 2020). The hierarchical cluster analysis technique enables an interconnection of samples according to their associations to produce an analysis dendrogram, through which

samples similar to the chosen variables can be grouped (Ferraz et al., 2014). It is useful to visualize similarities in samples and objects through a representation of points in space, which is not possible in classic graphics (Lau et al., 2009).

Results and discussion

The flight time, number of images, and processing times according to different superpositions and flight directions are presented in Table 4.

As shown in most results provided in Table 4, as the overlap increases, there is also an increase in data processing and flight time due to the higher number of images captured by the sensor. As described in a study by Mesas-Carrascosa et al. (2016), the increase in flight altitude within the same study area and overlay allows one to obtain a smaller amount of images of the studied area.

Regarding the flight plans, we observed that in smaller image overlaps, a shorter route was necessary to cover the area. However, in smaller overlaps, fewer images were captured; thus, each scene has greater coverage. The 90x90% and 80x80% overlap plans required longer flight times, resulting in higher battery consumption from the UAV (Table 4). In other flight missions, a pattern between 3 and 5 minutes prevailed. Shorter flight times were observed for less than 80% of overlaps. Thus, overlaps can be a significant factor in flight planning, given the possible variations in other parameters, such as flight time and image processing.

To evaluate the differences between topographic profiles (Figure 5), it is possible to observe the profile lines generated from the DTMs for the flight configuration in each direction (Longitudinal and Transverse) compared to those in the profile generated by the RTK survey (control).

In general, as the overlap percentage decreases, the profile elevation points show a higher deviation from the reference profile. Leitão et al. (2016)

determined that greater overlaps increase the redundancy of point identification and enhance image quality.

In the longitudinal direction (Figure 5A), the differences between lines and the point deviations from the control (GNSS RTK profile) were higher than those in the transverse direction (Figure 5B). The transverse direction presents better results when compared to the longitudinal direction because in this direction the flight occurred in the same direction as the area's ramp. The UAV used in this study has settings that do not follow the terrain elevation slope, so comparing the q direction coincides with the slope direction (transverse direction) yields better results. Moreover, based on an assessment of both figures of the two flight directions, the closest overlap to the reference is 90x90%, while the most inconsistent is 60x30%.

However, there are particular factors related to the flight direction. For example, in the longitudinal direction (Figure 5A), the 60x40% overlap profile was closer to the reference than some flight profiles with larger overlaps, such as the 70x50% profile. In the transverse direction (Figure 5B), the 70x50% overlap profile was promising, with behavior close to the control profile. It was also possible to verify that in the transverse direction the 60x40% profile seems to be better to the 70x30% profile, due to the influence of the lateral overlap in this direction. The transverse type flights to the ground surface are influenced by the percentage of lateral overlap being evidenced in these two flights. It is also noteworthy that the variations demonstrated when comparing the topographic profile to the profiles generated by the UAV can still be described as systematic errors. These are produced due to the image acquisition platform and the sensor that have errors associated both in the GPS configuration as well as considering different link points in each overlap and flight direction for the construction of the study products.

Table 4. Flight duration, numbers of generated images, and processing times under different overlaps and flight directions.

Flight Number	Overlap (%)	Direction	Flight time	Generate Images	Processing Time
1	90x90	Longitudinal	13 min 13 sec	231	2 hours 38 sec
2	80x80	Longitudinal	7 min 50 sec	65	41 min 09 sec
3	80x60	Longitudinal	4 min 04 sec	36	23 min 36 sec
4	80x60	Transverse	4 min 43 sec	34	22 min 44 sec
5	70x50	Longitudinal	3 min 47 sec	19	14 min 35 sec
6	70x50	Transverse	4 min 30 sec	20	12 min 17 sec
7	70x30	Longitudinal	4 min 33 sec	20	9 min 56 sec
8	70x30	Transverse	4 min 20 sec	18	10 min 18 sec
9	60x40	Longitudinal	4 min 26 sec	19	15 min 25 sec
10	60x40	Transverse	3 min 37 sec	18	18 min 10 sec
11	60x30	Longitudinal	4 min 33 sec	19	15 min 17 sec
12	60x30	Transverse	3 min 46 sec	18	10 min 47 sec

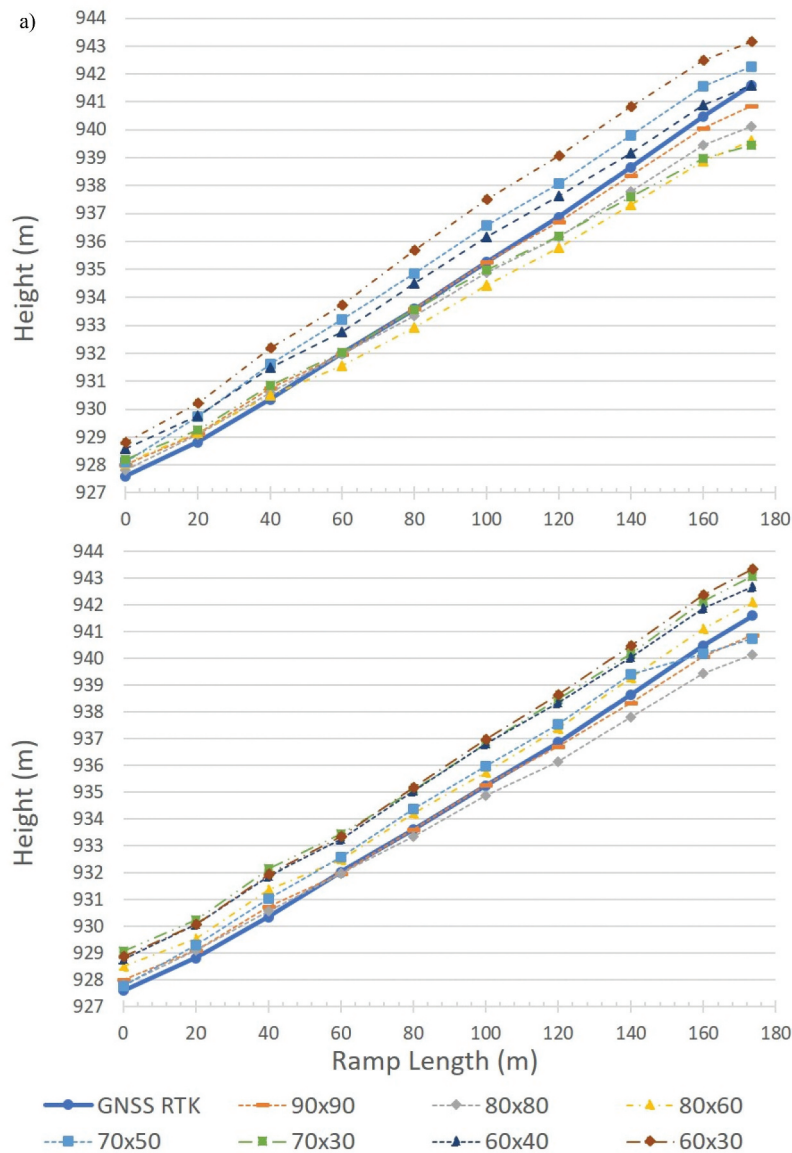


Figure 5. Comparison between the topographic profiles of the DTM generated by GNSS RTK and the DTMs produced from UAV images and their respective overlaps (in percentages), with the flights in the longitudinal direction A) and transverse direction B) to the crops.

The elevation differences between the profiles generated from the UAV data and the profile derived from the data surveyed by GNSS were calculated (in meters) to rank the discrepancies numerically and provide a better understanding of variations. The sums of squares (SQ) of these differences were also calculated. The results of this process are shown in Table 5.

As shown in the profiles generated from flights in the longitudinal direction, as the overlap decreases, the SQ values increases (Table 5). Dandois et al. (2015), in a study on the ideal flight conditions for computer-vision UAV estimations of forest structure, noted that during image processing, smaller overlaps decreased the dense point-cloud number, resulting in larger elevation errors. However, an exception was observed when comparing the control and 60x40% overlap, in which the values were lower than those under the same approach involving the 80x60%, 70x50%, and 70x30% overlaps.

Moreover, in the profiles from flights in the transverse direction (Table 5), there was no pattern observed in the increases in SQ difference associated with a decrease in overlap percentage, despite the close proximity of 90x90% (highest overlap) to the reference. Notably, the 70x50% overlap obtained a difference value smaller than 80x80% (with an SQ of 4.041 versus 4.877, respectively).

There is still a lack of scientific explanations for this observation. To solve this problem, the flights on the two trajectories could be combined, as done in the studies by Gerke and Przybilla (2016), who increased the precision of data obtained through a so-called “cross-flight”. Further, the most divergent values for both trajectories were obtained in the lowest overlap percentage (60x30%).

A Dunnett Test (at a significance level of $\rho = 0.05$) was performed to assess which DTMs topographic profile elevations showed a significant

Table 5. Elevation differences in meters (m) between DTMs produced with different overlaps (transverse and longitudinal flights to the crop) and the control profile obtained by GNSS RTK for each topographic profile.

Ramp section (m)	RTK -(90x90)%	RTK -(80x80)%	RTK -(80x60)%	RTK -(70x50)%	RTK -(70x30)%	RTK -(60x40)%	RTK -(60x30)%
LONGITUDINAL							
0,00	0,394	0,207	0,481	0,518	0,610	0,980	1,194
20,00	0,302	0,283	0,337	0,927	0,439	0,945	1,413
40,00	0,397	0,228	0,157	1,265	0,500	1,124	1,829
60,00	0,026	0,033	0,451	1,210	0,012	0,755	1,725
80,00	0,002	0,258	0,657	1,234	0,028	0,883	2,071
100,00	0,027	0,381	0,826	1,328	0,267	0,915	2,259
120,00	0,147	0,716	1,100	1,214	0,665	0,778	2,201
140,00	0,301	0,857	1,354	1,162	1,066	0,520	2,178
160,00	0,407	1,030	1,603	1,070	1,515	0,414	2,014
173,50	0,739	1,477	1,981	0,662	2,143	0,024	1,559
SQ	1,229	4,877	11,224	11,885	9,353	6,351	35,210
TRANSVERSE							
0,00	0,394	0,207	0,900	0,177	1,467	1,190	1,271
20,00	0,302	0,283	0,737	0,490	1,415	1,272	1,257
40,00	0,397	0,228	1,007	0,687	1,795	1,532	1,579
60,00	0,026	0,033	0,481	0,577	1,418	1,247	1,337
80,00	0,002	0,258	0,597	0,783	1,461	1,429	1,584
100,00	0,027	0,381	0,496	0,707	1,565	1,564	1,716
120,00	0,147	0,716	0,516	0,689	1,612	1,470	1,764
140,00	0,301	0,857	0,617	0,740	1,533	1,375	1,820
160,00	0,407	1,030	0,637	0,312	1,655	1,388	1,892
173,50	0,739	1,477	0,512	0,856	1,475	1,064	1,739
SQ	1,229	4,877	4,516	4,041	23,834	18,534	25,958

difference from the GNSS RTK control profile. The results are presented in Table 6 for the longitudinal and the transverse direction.

Based on the Dunnett Test, the results met our expectations since the DTMs profiles with greater overlaps, such as 90x90% and 80x80%, had the closest values to the topographic profile obtained using a topographic survey by GNSS RTK methodology. However, some smaller overlaps, such as 70x30% (longitudinal) and 70x50% (transverse), obtained good results and, therefore, also did not differ significantly from the reference. Notably, the 70x50% transverse overlap obtained values even closer to the control than the 80x80% overlap. Satisfactory results were also found by Beretta et al. (2018) in a study on DTMs in mining regions. The authors attested the high accuracy of photogrammetric techniques compared to RTK and laser scanner measurements, highlighting the high detail levels of photogrammetric DTMs.

In the topography method, the distance between the tracked points may not accurately represent fine details in the terrain. UAVs can enhance this method by providing a greater number of points, as pixels with elevation values are collected from over the entire surface with no need for interpolation, as is usually performed with GNSS RTK data.

Furthermore, the squared error was calculated by comparing the DTMs in their entirety to the control to assess changes in elevation over the entire terrain by comparing different topographic profiles. Table 7 shows the MSE and RMSE results for the studied area in

Table 6. Average elevation values in the central profiles obtained in the DTMs generated by the UAV data in meters (m) for flights in the longitudinal and transverse directions, including the contrasts between the control (profile produced via GNSS RTK) and the results of the Dunnett test (at a significance level of $p = 0.05$).

MTD overlap	Average profile Elevation (m)	Contrast from reference estimation	
LONGITUDINAL			
GNSS RTK	934.52	a	-
90x90%	934.47	a	0.05
80x80%	934.12	a	0.40
70x30%	934.11	a	0.41
80x60%	933.82	b	0.70*
60x40%	935.25	b	0.73*
70x50%	935.58	b	1.06*
60x30%	936.36	b	1.84*
TRANSVERSE			
GNSS RTK	934.52	a	-
90x90%	934.47	a	0.05
70x50%	935.58	a	0.37
80x80%	934.12	a	0.40
80x60%	933.82	b	0.65*
60x40%	935.25	b	1.35*
70x30%	934.11	b	1.54*
60x30%	936.12	b	1.60*

meters (m), based on the difference between the DTM generated using topographic survey (GNSS RTK), compared to the DTMs generated by the UAV. An average RMSE variation of 0.341 m (overlap, 90x90%) to 1.742 m (overlap 60x30% of longitudinal type) was observed.

In Figures 6 and 7, the MSE outlined in Table 7 is distributed over the studied terrain to visualize the behavior of this type of spatial error over the entire study area.

The longitudinal and transverse overlap settings with higher percentages resulted in lower error values for most UAV flights, except for the 70x50% transverse overlap, which showed lower errors than the higher overlaps.

Notably, we observed lower error values for longitudinal flights with greater overlaps of 90x90% and 80x80% compared to the flight directions for the same overlaps. The intermediate overlaps of 80x60% and 70x50% in the transverse flight direction presented lower error values than those in the longitudinal flight direction. All other overlaps presented lower errors in the longitudinal flight direction compared to those in the transverse flight direction.

Flight direction behavior affects image processing and DTMs generation. This occurred because the larger amount of information used to extract the tie points contributed to an increase in error.

Table 7. Mean squared error (MSE) and root mean square error (RMSE) in meters (m) for each flight plan studied.

Flight Plan	Overlap (%)	Direction	MSE	RMSE
1	90x90	Longitudinal	0.116	0.341
2	80x80	Longitudinal	0.258	0.508
3	80x60	Longitudinal	0.494	0.703
4	80x60	Transverse	0.402	0.634
5	70x50	Longitudinal	1.858	1.363
6	70x50	Transverse	0.347	0.589
7	70x30	Longitudinal	0.536	0.732
8	70x30	Transverse	1.071	1.035
9	60x40	Longitudinal	0.548	0.740
10	60x40	Transverse	2.235	1.495
11	60x30	Longitudinal	3.035	1.742
12	60x30	Transverse	2.427	1.558

In this study, however, a more precise flight direction was not determined, as the determined deviations and errors did not follow a pattern indicating the best direction to be adopted.

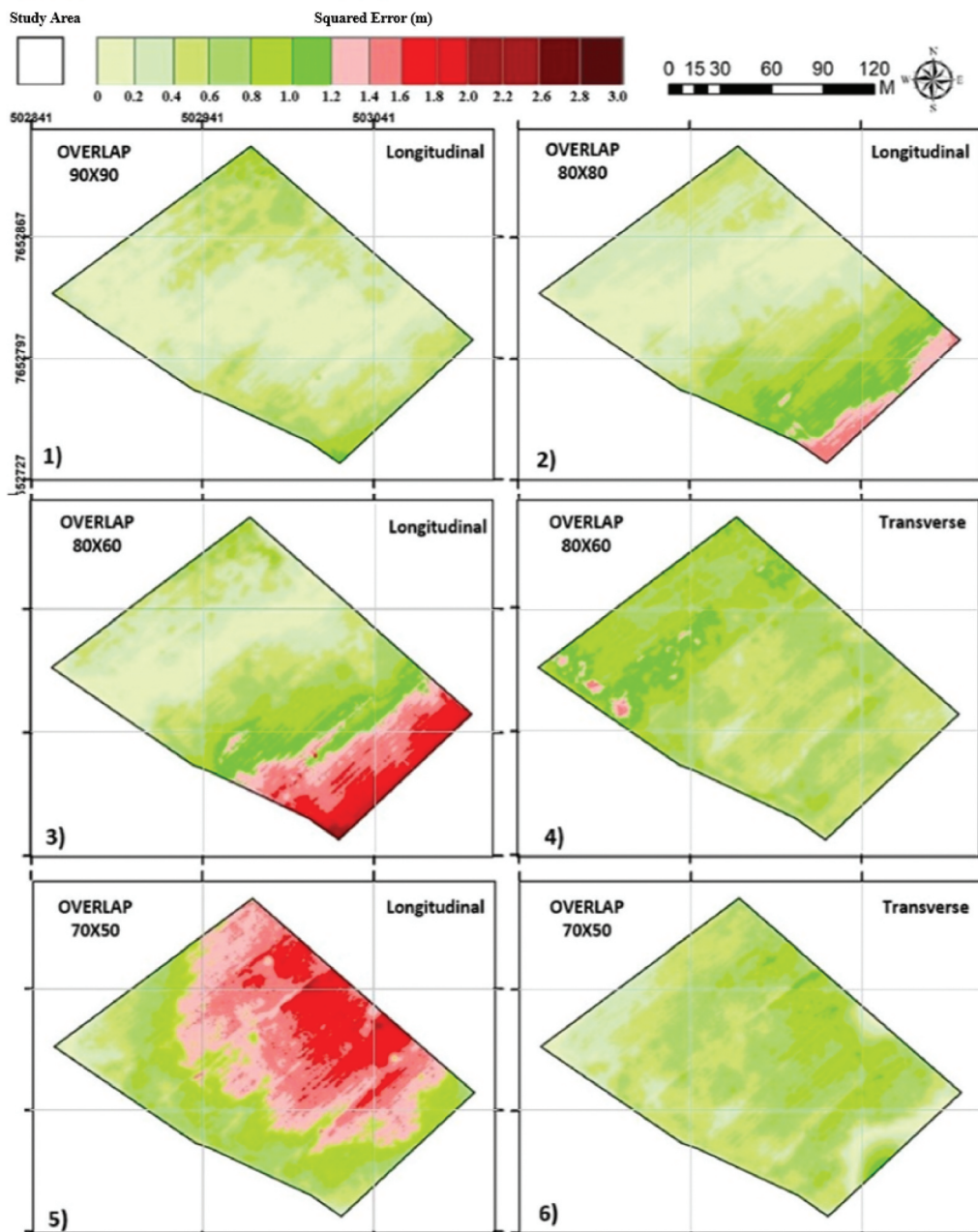


Figure 6. Squared error in meters (m) for flight plans (numbers indicate 1–6 flight plans).

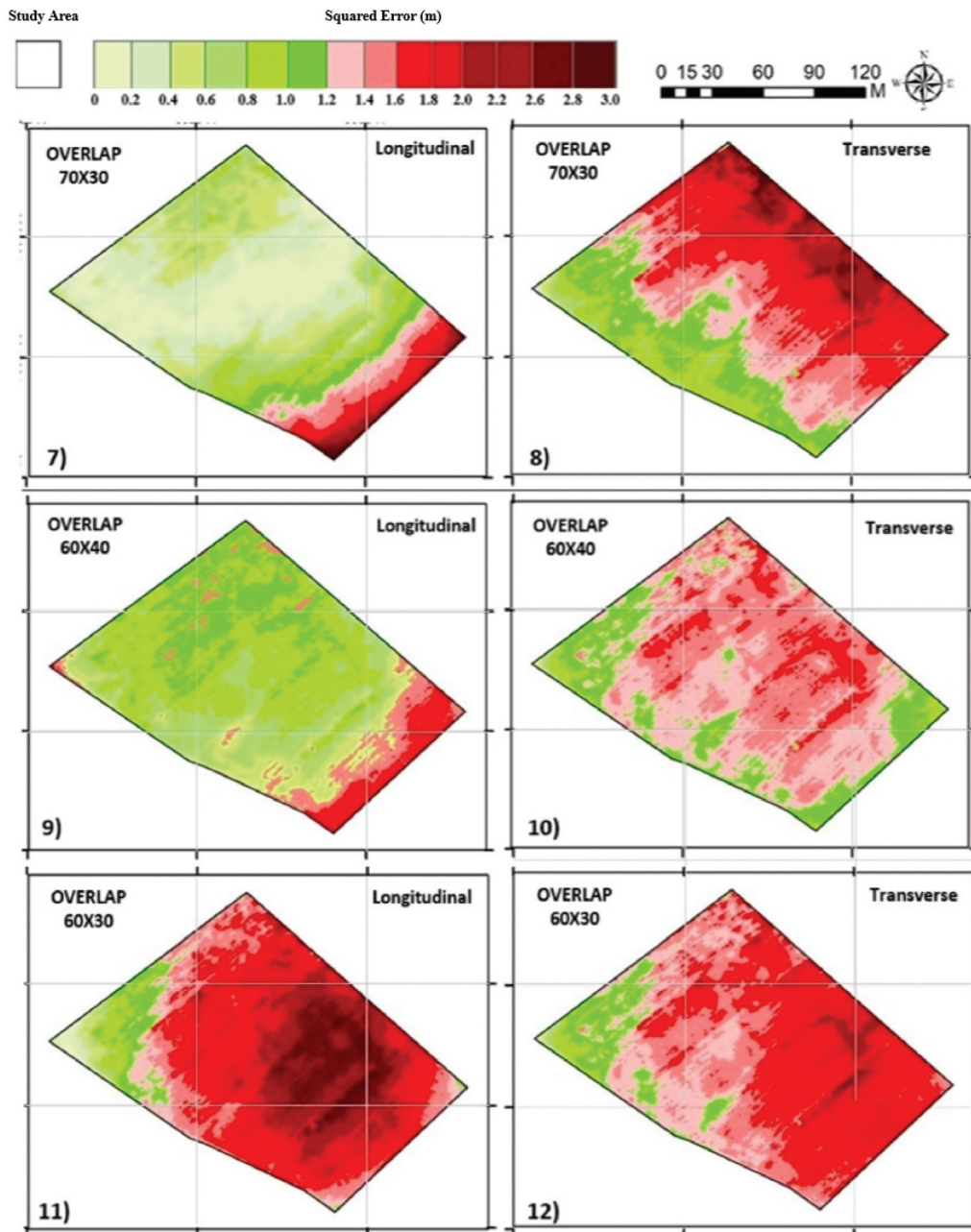


Figure 7. Squared error in meters (m) for flight plans (numbers indicate 7–12 flight plans).

The greatest overlaps (90x90% and 80x80%) resulted in minor associated errors. However, these overlaps required more time in flight and processing and produced a larger quantity of images for the sampled area. These requirements mean that the adoption of this type of overlap would not be a suitable option for aerial mapping compared to smaller overlaps, as the deviations related to such errors are not high.

Thus, it is relevant to verify the statistical similarities that can determine minor overlaps that meet the advantages of mapping with satisfactory errors. These overlaps should be statistically equal

to larger overlaps, with shorter flights and processing times. For this purpose, an agglomerative hierarchical analysis of dendrograms (clusters) was carried out to assess the behavior of the RMSEs obtained by comparing the UAV DTMs in their entirety with the control. The result is illustrated in Figure 8.

According to the distance scale, the dendrogram analysis resulted in a final partition of three groups containing four observations and components considered statistically equal. Analysis using the cophenetic correlation is commonly performed to establish a correlation between the values of the initial similarity matrix and those derived from the dendrogram. In

this study, a value of 0.867 was obtained, which indicates a good correlation and allows for reliable graphical interpretations (Rohlf & Fisher, 1968).

In Figure 8, the upper cluster has the longest distance on the scale and, consequently, the highest RMSE values. The lower cluster has an intermediate distance on the scale. The intermediate cluster has the shortest distance on the scale and includes the best-studied overlap (90x90) with the lowest RMSE value. The other overlaps are statistically equal within the same grouping, which demonstrates that the intermediate group contains the components with the fewest errors, indicating suitability for use. According to information from the manufacturer of the UAV used in this study, the inner GNSS system that guides the plane and the aerial image acquisition have a geographic positioning error of 0.5 m, thus, it is not possible to find error values below the error of the instrument of the UAV, that is, the values found in this study meet the proposed objective. Therefore, although the DTMs from smaller overlaps and with different flight directions can result in errors (sometimes statistically equal and sometimes slightly higher than those caused by DTMs from greater overlaps (90x90% and 80x80%), this factor does not prevent the use of such DTMs in mapping areas since the results remain close to those obtained using the topography method (GNSS RTK). These overlaps also

presented shorter flight and processing times and generated fewer images, guaranteeing battery savings and time optimization in the field, thereby representing an advantage in choosing this overlap over others.

Considering all the surveys proposed in this study, we determined that the 70x50% transverse overlap does not differ statistically from the higher overlaps of 90x90% and 80x80%, which include the minor errors determined in the study of the altimetric profiles and in the study of the DTMs RMSEs. Therefore, the 70x50% overlap stands out as the best flight plan evaluated in this work. This choice is based primarily on the shorter flight time of this overlap (4 minutes and 30 seconds), its low processing time (12 minutes and 17 seconds), and its low errors (0.588 m) produced in the mapped area, and also considers the minimum overlapping requirement of aerophotogrammetry.

Conclusion

The 70x50% transverse overlap provided reliable products with fewer time requirements in flight and data processing. In addition, the number of aerial images for this overlap was satisfactory for area coverage, with no statistically significant differences compared to the highest overlaps (90x90% and 80x80%) and fewer associated errors, both in

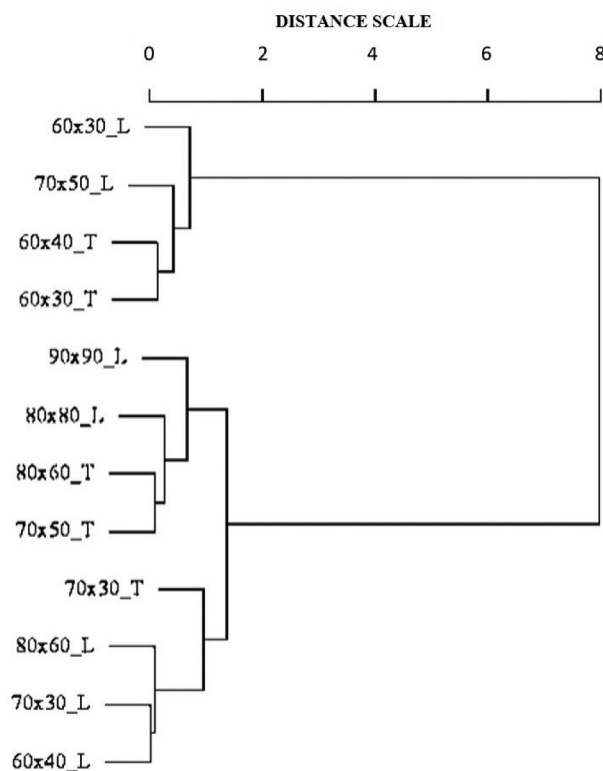


Figure 8. RMSE dendrogram of the 12 overlays and directions. *legend: _L: longitudinal; _T: transverse.

the study of the method (GNSS RTK) (using central topographic profiles) and in the overall surface evaluation approach, where considerations resulted from the RMSE analysis of the DTMs. The use of aerial images obtained by the UAV proved to be effective in imaging the area, resulting in a rapid survey that generated the DTMs as a product with reduced errors. The present study, therefore, addresses an important theme when designing UAV research to support the survey of land information in way that is optimized for both time and cost and can be applied to different activities in, e.g. the civil, agricultural, and environmental fields to ensure precision in decision making.


Acknowledgments

This work was supported by the Foundation for Research of the State of Minas Gerais (FAPEMIG), the National Council for Scientific and Technological Development (CNPq), the Coordination for the Improvement of Higher Education Personnel (CAPES), the Federal University of Lavras (UFLA), and the University of Firenze (UniFI).

Disclosure statement

No potential conflict of interest was reported by the author(s).

ORCID

Professor Gabriel Araújo E Silva Ferraz  <http://orcid.org/0000-0001-6403-2210>

Mr Lucas Santos Santana  <http://orcid.org/0000-0001-7489-3225>

Dr Leonardo Conti  <http://orcid.org/0000-0002-4181-5893>

Dr Giuseppe Rossi  <http://orcid.org/0000-0003-0211-9294>

References

- Aguilar, F. J., Agüera, F., Aguilar, M. A., & Carvajal, F. (2005). Effects of terrain morphology, sampling density, and interpolation methods on grid DEM accuracy. *Photogrammetric Engineering and Remote Sensing*, 71(7), 805–816. <https://doi.org/10.14358/PERS.71.7.805>
- Alvares, C. A., Stape, J. L., Sentelhas, P. C., De Moraes, G., Leonardo, J., & Sparovek, G. (2013). Koppen's climate classification map for Brazil. *Meteorologische Zeitschrift*, 22(6), 711–728. <https://doi.org/10.1127/0941-2948/2013/0507>
- Barbosa, E. D. M., Monico, J. F. G., Alves, D. B. M., & De Oliveira, L. C. (2013). Integrity in RTK and network RTK positioning. *Brazilian Geodesic Science Bulletin*, 16(4), 589–605. <https://doi.org/10.1590/S1982-21702010000400007>
- Beretta, F., Shibata, H., Cordova, R., Peroni, R. D. L., Azambuja, J., & Costa, J. F. C. L. (2018). Topographic modeling using UAVs compared with traditional survey methods in mining. *International Engineering Journal*, 71(3), 463–470. <https://doi.org/10.1590/0370-44672017710074>
- Burrough, P. A., & McDonnell, R. A. (1998). *Principles of GIS*. Oxford University Press.
- Clapuyt, F., Vanacker, V., & Van Oost, K. (2016). Reproducibility of UAV-based earth topography reconstructions based on structure-from-motion algorithms. *Geomorphology*, 260, 4–15. <https://doi.org/10.1016/j.geomorph.2015.05.011>
- D'Andréa, A. F., Silva, M. L. N., Curi, N., Freitas, D. A. F. D., Roscoe, R., & Guimarães, P. T. G. (2009). Short-term variations of soil CO₂ emissions in coffee plantations. *Química Nova, São Paulo*, 32(9), 2314–2317. <https://doi.org/10.1590/S0100-40422009000900014>
- Dandois, J., Olano, M., & Ellis, E. (2015). Optimal altitude, overlap, and weather conditions for computer vision UAV estimates of forest structure. *Remote Sensing*, 7(10), 13895–13920. <https://doi.org/10.3390/rs71013895>
- Dunnnett, C. W. (1995). A multiple comparison procedure for comparing several treatments with a control. *Journal of the American Statistical Association*, 272(50), 1096–1121. <https://doi.org/10.1080/01621459.1955.10501294>
- Eisenbeiss, H. (2009). UAV Photogrammetry [Doctor of Sciences Thesis]. University of Technology Dresden; p. 2009.
- Eltner, A., Kaiser, A., Abellan, A., & Schindewolf, M. (2017). Time lapse structure-from-motion photogrammetry for continuous geomorphic monitoring. *Earth Surface Processes and Landforms*, 42(14), 2240–2253. <https://doi.org/10.1002/esp.4178>
- Esri. *ArcGIS: Software 10.1*. (2013). <https://www.esri.com>
- Ferraz, P. F., Yanagi Junior, T., Alvarenga, T. A., Reis, G. M., & Campos, A. T. (2014). Behavior of chicks subjected to thermal challenge. *Agricultural Engineering, Jaboticabal*, 34(6), 1039–1049. <https://doi.org/10.1590/S0100-69162014000600002>
- Gerke, M., & Przybilla, H. J. (2016). Accuracy analysis of photogrammetric uav image blocks: Influence of onboard rtk-gnss and cross flight patterns. *Photogrammetrie - Fernerkundung - Geoinformation*, 1(1), 17–30. 2016. <https://doi.org/10.1127/pfg/2016/0284>
- Hallak, R., & Pereira, F. (2011). Methodology for performance analysis of simulations of convective systems in the metropolitan area of São Paulo with the ARPS model: Sensitivity to variations with the advection and the data assimilation schemes. *Brazilian Journal of Meteorology*, 26(4), 591–608. <https://doi.org/10.1590/S0102-77862011000400009>
- Hashemi-Beni, L., Jones, J., Thompson, G., Johnson, C., & Gebrehiwot, A. (2018). Challenges and opportunities for uav-based digital elevation model generation for flood-risk management: A case of princeville, north carolina. *Sensors*, 18(11), 3843. <https://doi.org/10.3390/s18113843>
- Hirschmuller, H. (2007). Stereo processing by semiglobal matching and mutual information. *IEEE Transactions on Pattern Analysis and Machine Intelligence*, 30(2), 328–341. <https://doi.org/10.1109/TPAMI.2007.1166>

- Höhle, J. (2009). DEM generation using a digital large format frame camera. *Photogrammetric Engineering and Remote Sensing*, 75(1), 87–93. <https://doi.org/10.14358/PERS.75.1.87>
- Klemas, V. V. (2015). Coastal and environmental remote sensing from unmanned aerial vehicles: An overview. *Journal of Coastal Research*, 315(5), 1260–1267. <https://doi.org/10.2112/JCOASTRES-D-15-00005.1>
- Lau, J., Hung, W. T., & Cheung, C. S. (2009). Interpretation of air quality in relation to monitoring station's surroundings. *Atmospheric Environment, Oxford*, 43(4), 769–777. <https://doi.org/10.1016/j.atmoenv.2008.11.008>
- Leachtenauer, J. C., & Driggers, R. G. (2001). *Surveillance and reconnaissance imaging systems: Modeling and performance prediction*. Artech House.
- Leitão, J. P., De Vitry, M. M., Scheidegger, A., & Rieckermann, J. (2016). Assessing the quality of digital elevation models obtained from mini unmanned aerial vehicles for overland flow modelling in urban areas. *Hydrology and Earth System Sciences*, 20(4), 1637–1653. <https://doi.org/10.5194/hess-20-1637-2016>
- Mesas-Carrascosa, F. J., Notario García, M. D., Meroño De Larriva, J. E., & García-Ferrer, A. (2016). An analysis of the influence of flight parameters in the generation of unmanned aerial vehicle (UAV) orthomosaics to survey archaeological areas. *Sensors*, 16(11), 11. 1838. <https://doi.org/10.3390/s16111838>
- Mora, O. E., Chen, J., Stoiber, P., Koppányi, Z., Pluta, D., Josenhans, R., & Okubo, M. (2020). Accuracy of stockpile estimates using low-cost sUAS photogrammetry. *International Journal of Remote Sensing*, 41(12), 4512–4529. <https://doi.org/10.1080/01431161.2020.1723167>
- Peña, J. M., Torres-Sánchez, J., De Castro, A. I., Kelly, M., & López-Granados, F. (2013). Weed mapping in early-season maize fields using object-based analysis of unmanned aerial vehicle (UAV) images. *PloS one*, 8(10), 77151. <https://doi.org/10.1371/journal.pone.0077151>
- Pereira, O. J. R., Tamamaru, R., & Centenário, A. (2013). Geração de modelos digitais de elevação com base em técnicas de estereoscopia digital, por meio de imagens VANT: Subsídio a identificação de manchas de desmatamento em áreas de preservação permanente. *Simpósio Brasileiro De Sensoriamento Remoto*, 16, 2113–2119.
- R Development Core Team. 2020. *R: A language and environment for statistical computing*. R Foundation for Statistical Computing. 3. 3900051070. <900051070. <<http://www.R-project.org/>>
- Rabah, M., Basiouny, M., Ghanem, E., & Elhadary, A. (2018). Using RTK and VRS in direct geo-referencing of the UAV imagery. *NRIAG J. Astron Geophys*, 7(2), 220–226. <https://doi.org/10.1016/j.nrjag.2018.05.003>
- Rohlf, F. J., & Fisher, D. L. (1968). Test for hierarchical structure in random data sets. *Systematic Zoology, Washington*, 17(4), 407–412. <https://doi.org/10.2307/2412038>
- Rumpler, M., Wendel, A., & Bischof, H. (2013). Probabilistic range image integration for DSM and true-orthophoto generation. *Springer*, 7944, 533–544. https://doi.org/10.1007/978-3-642-38886-6_50
- Santana, L. S., Ferraz, G. A. S., Santos, L. M., Maciel, D. A., Barata, R. A. P., Reynaldo, E. F., & Rossi, G. (2019). Vegetative vigor of maize crop obtained through vegetation indexes in orbital and aerial sensors images. *Brazilian Journal of Biosystems Engineering*, 13(3), 195–206. <http://dx.doi.org/10.18011/bioeng2019v13n3p195-206>
- Santos, L. M., Ferraz, G. A. S., Andrade, M. T., Santana, L. S., Barbosa, B. D. S., Maciel, D. T., & Rossi, G. (2019). Analysis of flight parameters and georeferencing of images with different control points obtained by RPA. *Agronomy Research*, 17, 2054–2063. <https://doi.org/10.15159/AR.19.173>
- Santos, L. M., Ferraz, G. A. E. S., Barbosa, B. D. D. S., Diotto, A. V., Maciel, D. T., & Xavier, L. A. G. (2020). Biophysical parameters of coffee crop estimated by UAV RGB images. *Precision Agriculture*, 21, 1–15. <https://doi.org/10.1007/s11119-020-09716-4>
- Silva, C. A., Duarte, C. R., Dos Santos, A. L. S., Amaro, V. E., Bicho, C. P., & Sabadia, J. A. B. (2016). Evaluating the accuracy in volume calculation in a pile of waste using UAV, GNSS and LiDAR. *Brazilian Geodesic Science Bulletin*, 22, 1982–2170. <https://doi.org/10.1590/S1982-21702016000100005>
- Smith, M. W., Carrivick, J. L., & Quincey, D. J. (2016). Structure from motion photogrammetry in physical geography. *Progress in Physical Geography*, 40(2), 247–275. <https://doi.org/10.1177/0309133315615805>
- Sopchaki, C. H., Da Paz, O. L. D. S., De Salles Graça, N. L. S., & Sampaio, T. V. M. (2018). Verificação da qualidade de ortomosaicos produzidos a partir de imagens obtidas com aeronave remotamente pilotada sem o uso de pontos de apoio. *Raega-O Espaço Geográfico em Análise*, 43, 200–214. <https://doi.org/10.5380/raega>
- Tamminga, A., Hugenholtz, C., Eaton, B., & Lapointe, M. (2015). Hyperspatial remote sensing of channel reach morphology and hydraulic fish habitat using an unmanned aerial vehicle (UAV): A first assessment in the context of river research and management. *River Research and Applications*, 31(3), 379–391. <https://doi.org/10.1002/rra.2743>
- Torrado, J. O. E., Jiménez, J. J. C., & Díaz, H. P. (2016). Orthomosaics and digital elevation models generated from images taken with UAV systems. *Tecnura*, 20(50), 119–140. <http://dx.doi.org/10.14483/udistrital.jour.tecnura.2016.4.a09>
- Torres-Sánchez, J., Pena, J. M., De Castro, A. I., & López-Granados, F. (2014). Multi-temporal mapping of the vegetation fraction in early-season wheat fields using images from UAV. *Computers and Electronics in Agriculture*, 103, 104–113. <https://doi.org/10.1016/j.compag.2014.02.009>
- Uysal, M., Toprak, A. S., & Polat, N. (2015). DEM generation with UAV photogrammetry and accuracy analysis in Sahitler hill. *Measurement. Journal of the International Measurement Confederation*, 73, 539–543. <https://doi.org/10.1016/j.measurement.2015.06.010>
- Vitti, D. M. C., Júnior, C. B., Mauad, F. F., & Veronez, M. R. (2017). Determinação das componentes do desvio da vertical para estabelecimento de referencial batimétrico na Represa do Lobo, Itirapina-SP. *Revista Brasileira de Cartografia*, 69, 253–261.

Westoby, M. J., Brasington, J., Glasser, N. F., Hambrey, M. J., & Reynolds, J. M. (2012). 'Structure-from-motion' photogrammetry: A low-cost, effective tool for geoscience applications. *Geomorphology*, 179, 300–314. <https://doi.org/10.1016/j.geomorph.2012.08.021>

Zisi, T., Alexandridis, T. K., Kaplanis, S., Navrozidis, I., Tamouridou, A. A., Lagopodi, A., Moshou, D., & Polychronos, V. (2018). Incorporating surface elevation information in UAV multispectral images for mapping weed patches. *Journal of Imaging*, 4(11), 132. <https://doi.org/10.3390/jimaging4110132>